# Novel Styrene-Based Polyamine Sorbent for Efficient Selective Separation of Molybdenum

Fan Guo, Xiaoli Xi,* Liwen Ma, and Zuoren Nie

Read Online

ACCESS | 📊 Metrics & More | 📰 Article Recommendations | 🔬 Supporting Information

**ABSTRACT:** Tungsten (W) and molybdenum (Mo) are important strategic resources but the two coexist in both primary ore and waste. Before a single metal product is obtained, it is often necessary to separate the two. In this work, we reported two new polyamine resins (D301@PA and D301@TA), which can be obtained by an assembled amine (primary amine or tertiary amine) and traditional D301 resin by the dipping method. Then, the sorption experiments with the amine resins were carried out, and the selectivity and sorption capacity of the two new polyamine resins for $MoS_4^{2-}$ have been significantly improved. Among them, D301@TA showed the highest sorption capacity of 414 mg·g$^{-1}$ and a separation factor of 108. Finally, the sorption mechanism can be inferred through scanning electron microscopy (SEM), Brunauer−Emmett−Teller (BET) analysis, and X-ray photoemission spectroscopy (XPS); the Cl$^-$ ions in the amine resin and the $MoS_4^{2-}$ ions were subjected to ion exchange. This work provides a green and efficient approach for separating tungsten and molybdenum.
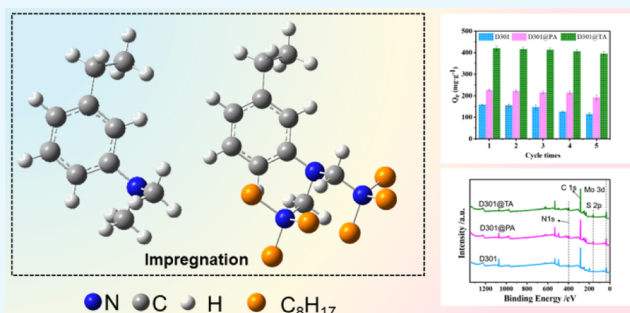
## INTRODUCTION

With the increase of the global population and the continuous economic growth of developing countries, the demand for energy is increasing worldwide, especially the refractory metals tungsten and molybdenum required in production and life. Recently, increasing attention has been paid to the recycling of the secondary resources of tungsten and molybdenum.[1] The recovery of tungsten and molybdenum secondary resources can not only reduce the environmental pollution caused by stacking but also effectively supplement the tungsten or molybdenum mineral resources and reduce the damage to the environment during the mining of mineral resources.[2] Typical secondary resources of tungsten include tungsten slag, alloy scraps,[3] and waste catalysts containing tungsten,[4] but they are often accompanied by molybdenum because of their similar properties. Due to the purity requirements of tungsten products, the separation of tungsten and molybdenum has become a necessary part in the production process.[5,6] In particular, the industrial feed solution contains 30−160 g·L$^{-1}$ WO$_3$ and 1−3 g·L$^{-1}$ Mo, which has a serious negative impact on the quality of tungsten products and causes the waste of molybdenum resources.[5]

To date, many techniques have been used to selectively remove molybdenum from tungstate solutions, which mainly include wet separation[6−8] and solid-phase sorption.[9] Traditional tungsten and molybdenum secondary resource recovery technology is based on solvent extraction technology,[7,10] which involves large material and energy consumption and produces organic waste liquid, waste gas, and other secondary pollution.

Obviously, solid-phase sorption[11,12] (porous resin and carbon material) is simple, reliable, and efficient. So far, various porous materials such as porous resins, activated carbon, etc., used to adsorb molybdenum have been studied. The porous resin formed by the strong interaction between a macroporous weakly basic resin matrix and a nitrogen-containing functional group is the most common sorbent in tungsten production.[13] It is a promising sustainable separation technology for tungsten and molybdenum.

The application of styrene-based resins for separation of tungsten and molybdenum is low cost and environmentally friendly. To further improve the selectivity and sorption capacity of resins, a series of resins with styrene-based functional groups through chemical modification, impregnation, and other different methods were prepared. Due to the excellent affinity between N and C, the amine functional group can be assembled on the styrene matrix through a chemical reaction. For example, Cr has been recovered with a poly-epichlorohydrin-dimethylamine-modified (EPIDMA-modified) D301 resin.[14] Thus, to improve the absorption capacity, the functional group could be modified.[15,16] These experiments
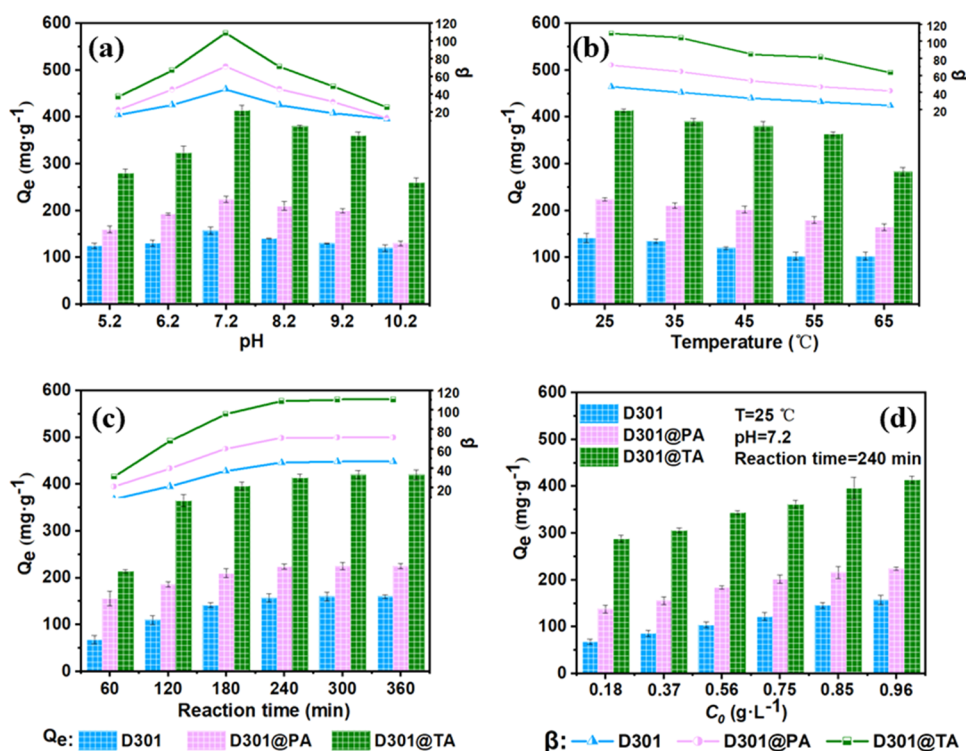
**Figure 1.** Effect of the (a) pH value, (b) reaction temperature, (c) contact time, and (d) raw concentration of Mo in the solution on sorption capacity ($Q_e$) and separation factor ($\beta$).

show that the resin's selective sorption to metal ions is mainly caused by the amino group in the resin; the longer the carbon chain contained in the amino group, the greater the steric hindrance, resulting in better selectivity. However, the number of sorption sites that can be provided by each single resin molecule is limited, and the amino group sneaks into the depth of the resin's pore size and cannot effectively contact the molybdenum molecule. Therefore, it is urgent to develop a novel styrene-based polyamine sorbent for efficient selective separation of molybdenum. Recently, primary amines (PAs) and tertiary amines (TAs) have attracted enormous attention owing to their excellent properties used for separation of tungsten and molubdenum.[6,17]

In this study, to solve the above-mentioned shortcomings of the styrene matrix and to further explore and study the sorption performance and influence of different amino groups on $MoS_4^{2-}$ anions, we prepared two kinds of new polyamine sorption materials (D301@TA and D301@PA). The aims of separating tungsten and molybdenum can effectively be achieved. Sorption−desorption experiments confirmed the sustainability and cost-effectiveness. In comparison to other similar adsorbents, the resin has advantages of easy preparation, low cost, high sorption capacity, and environmentally friendly. Finally, the sorption mechanism was thoroughly analyzed through SEM, BET analysis, and XPS.

## ■ RESULTS AND DISCUSSION

**Sorption Properties.** To evaluate the sorption performances of D301, D301@PA, and D301@TA for $MoS_4^{2-}$, a series of experiments were performed under different conditions, and the results are shown in Figure 1. The relevant experimental data are shown in Tables S1−S4 in the Supporting Information. First, the pH value of the tungstate solution was adjusted by adding diluted hydrochloric acid or sodium

hydroxide. As shown in Figure 1a, D301, D301@PA, and D301@TA can remove $MoS_4^{2-}$ effectively in a wide pH range (from 5.2 to 10.2). $Q_{Mo}$ increased with the increase of the pH value until it exceeded 7.2. Then, upon further increasing the pH value, the $Q_{Mo}$ value decreased because $H^+$ ions in the solution saturated $MoS_4^{2-}$ anions under acidic conditions, thereby reducing the sorption capacity of the adsorbent. As the pH value increased, the concentration of $OH^-$ in the solution increased. Since the electron-donating ability of $OH^-$ is stronger than that of $MoS_4^{2-}$, N atoms in the resin will be preferentially saturated by $OH^-$ rather than $MoS_4^{2-}$. Thus, a pH value of 7.2 was selected as the working condition. The reaction temperature also changed the sorption capacity. As shown in Figure 1b, with an increase in the temperature from 25 to 75 °C, the sorption capacity of resins for Mo slowly decreased. Considering both the sorption capacity and the separation factor, a reaction temperature of 25 °C might be appropriate for the sorption process.

As shown in Figure 1c, the sorption capacities and separation factors of D301, D301@PA, and D301@TA increased as the contact time increased at 25 °C. It was observed that the sorption capacity increased for $MoS_4^{2-}$ as the reaction time increased from 0 to 150 min and then became constant. In the follow-up mechanism analysis, saturation of the active sites (N) in resins and electron transfer between adsorbents and $MoS_4^{2-}$ anions occurred. The active sites (N) were dominant for 60 min, so the sorption capacity increased rapidly. After the reaction of active sites was completed, the adsorbent continued to play its role, and the quality of the adsorbent was still increasing slowly until it reached an equilibrium. As shown in Figure 1d, we changed the mass of Mo in the raw solution to simulate different Mo concentration environments and controlled the reaction temperature at 25 °C; the contact time was 4 h. The results showed that the

maximum sorption capacities of $MoS_4^{2-}$ by D301, D301@PA, and D301@TA were 157, 224, and 414 mg·g$^{-1}$, and the separation factors were 45, 71, and 108, respectively.

As shown in Figure 1, when PA or TA was loaded on D301, its sorption capacity to $MoS_4^{2-}$ became higher than that of D301, especially in the case of TA, which is 257 mg·g$^{-1}$ higher than that of D301, indicating that the proposed amine resin exhibited high sorption capacity and high selectivity to $MoS_4^{2-}$. Finally, as shown in Figure 2, we summarized some typical
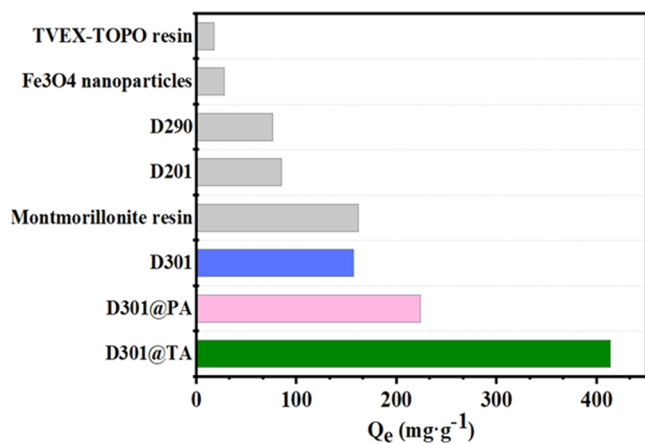


**Figure 2.** Comparison of the sorption capacity of some typical sorbents.

molybdenum adsorbents[18] and several typical styrene-based adsorbents.[19−22] Obviously, compared with other molybdenum adsorbents materials, styrene-based materials have unique advantages in terms of $MoS_4^{2-}$ sorption capacity. Among the styrene-based materials, our reported D301 resins showed the best high capacity. Moreover, as purely organic solid materials, they are more conducive to the subsequent long-term storage, and their production cost is lower.

**Structures.** To study the adsorption mechanism of the adsorbents, the structures of the adsorbents were determined by solid nuclear magnetism. Figure 3 shows the solid-state $^{13}$C

results of D301, D301@PA, and D301@TA. The peak position shows a little change because the relative content of the N-containing functional group is small, which can still explain the changes in the molecular structures before and after modification. In the solid phase, the characteristic peak at 128.5 ppm can be assigned to the benzene ring of the resin. In addition, the peaks at 145 ppm are attributed to the carbons ($-CH_2CH_3-$) in the benzene ring. These were observed in the resin before and after modification, indicating that the benzene ring structure is stable. The peaks at 43 and 65.5 ppm can be assigned to the functional groups containing N. Based on this, the molecular structural formulas of the three resins can be inferred. The different sorption capacities of the three resins for molybdenum in the solution drawn from Figure 1 may be mainly caused by the different structures of their N-containing functional groups. In summary, the above results show that the sorption performance of the resins is closely related to their molecular structures.

To further study the relationship between the molecular structure and sorption performance, first-principles calculations were employed to explore the relationship at a nanoscale. For these calculations, density functional theory (DFT) was used,[23−25] and the molecular structures were based on the results of NMR analysis. To establish the relationship between the molecular structure and analytical properties, it is necessary to perform optimization calculations on the structure. As shown in Figure 4, the optimized structures of D301, D301@PA, and D301@TA were obtained under the generalized gradient approximation (GGA), and the exchange−correlation functional of the calculation process uses the PBE functional. The resins, well known as anion exchange materials, have more active highest occupied molecular orbitals (HOMOs). According to frontier orbital theory, the smaller the absolute value of the energy difference between the HOMO of one reactant and the lowest unoccupied molecular orbital (LUMO) of another reactant ($\Delta E$), the more favorable is the interaction between the two. The efficiency of the amine resin as an adsorbent for $MoS_4^{2-}$ (donor and back-donor) depends on the ability to donate electrons and the tendency to
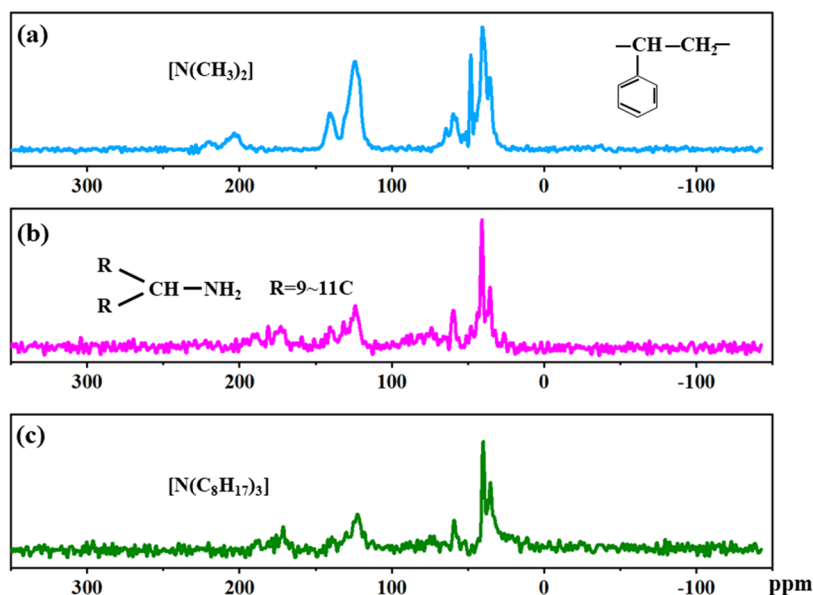


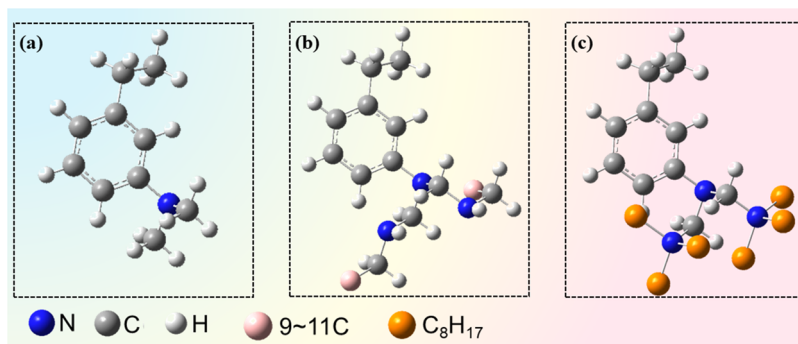**Figure 3.** $^{13}$C spectra of (a) D301, (b) D301@PA, and (c) D301@TA.

**Figure 4.** Optimized structures of (a) D301, (b) D301@PA, and (c) D301@TA obtained by MS DMol3.

accept them. Accordingly, it becomes necessary to discuss $\Delta E$. The reaction energy of the resin with $MoS_4^{2-}$ was calculated according to eq 1, and the results are shown in Table 1.

$$\Delta E = |E_{HOMO}^{resin} - E_{LUMO}^{MoS_4^{2-}}| \tag{1}$$

**Table 1. $\Delta E$ Data Based on Frontier Orbital Theory**

| model | LUMO (Ha) | HOMO (Ha) | $\Delta E$ (Ha) |
|---|---|---|---|
| D301 resin | −0.639 | −4.407 | 4.300 |
| PA resin | −0.338 | −0.919 | 0.812 |
| TA resin | −0.166 | −0.326 | 0.219 |
| $MoS_4^{2-}$ | −0.107 | −0.180 | |

where $E_{HOMO}^{resin}$ refers to the HOMO energy of the resin of the model compound, and $E_{LUMO}^{MoS_4^{2-}}$ refers to the LUMO energy of the model compound of $MoS_4^{2-}$.

According to Table 1, the results show that the $\Delta E$ values (0.812 and 0.219 Ha in solution) are relatively small, especially that of D301@TA, illustrating that it is easier to adsorb molybdenum in solution. Both the above trend of $\Delta E$ and the HOMO orbital value are consistent with that of the sorption performances in Figure 1, indicating that the lower energy may be one of the reasons for the excellent selectivity of resin molecules to Mo. In conclusion, different resin molecules form different morphologies, and the intrinsic energy values are determined by the different molecular structures, resulting in different adsorption properties. At the same time, this work realized the modification of D301 resin, the adsorption capacity, and the ability to donate electrons; D301@TA was better than D301@PA.

**Morphology.** To further understand the changes in the morphology of the resin before and after modification, Figure 5 shows the morphologies of D301, D301@PA, and D301@TA. For D301, from Figure 5a, it can be clearly seen that the resin is composed of macropores and columnar cross-linked pores. After modification, the macropores disappeared significantly.

For D301@PA, as shown in Figure 5b, almost all of the macropores disappeared and a more aggregated pore structure appeared. It can be seen more clearly in Figure 5c that the resin surface of D301@TA after TOA modification becomes a regular pore structure. Compared with D301, the surface morphology and pore structure of D301@PA and D301@TA are more regular, especially those of D301@TA, which is more conducive to sorption of $MoS_4^{2-}$ ions with a radius of 0.330 nm, and that can well explain the excellent sorption capacity of D301@TA.

**Specific Surface Area and Pore Size Distribution.** The specific surface area and pore size distribution of D301, D301@PA, and D301@TA were analyzed by the $N_2$ adsorption−desorption isotherm and the BJH model, and the results are shown in Figure 6. According to the calculations of BET and BJH, the specific surface area of pure D301 is 26.735 $m^2 \cdot g^{-1}$ and the pore size distribution is mainly concentrated at 17.510 nm. However, when the surface of pure D301 was coated with PA and TA aminating agents, the specific surface areas of the two modified adsorbents decreased to different degrees, corresponding to 25.341 and 22.981 $m^2 \cdot g^{-1}$, respectively, and the pore size distribution also changed. The reasons for the different pore size distributions are presented as follows: First, combined with the SEM analysis mentioned before, it can be more easily understood that compared with pure D301, the modified D301 surface was covered with a layer of the aminating agent, which blocked the original pores and channels, thereby reducing the specific surface area and pores. Second, PA and TA have stretchable carbon chains and they can combine with D301 through bonding during the preparation process, and the carbon chains are bent to increase the pore size distributions of D301@PA and D301@TA (Figure 6d−f). As shown in Figure 6d−f, it is obvious that all three are in the range of mesopores (2−50 nm), and their pore size is significantly larger than the radius of the $MoS_4^{2-}$ anion (0.330 nm). Therefore, the sorption of the resin to $MoS_4^{2-}$ is not only the surface coverage of the sorbent
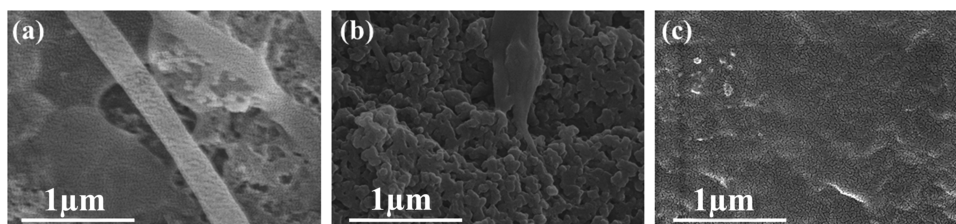


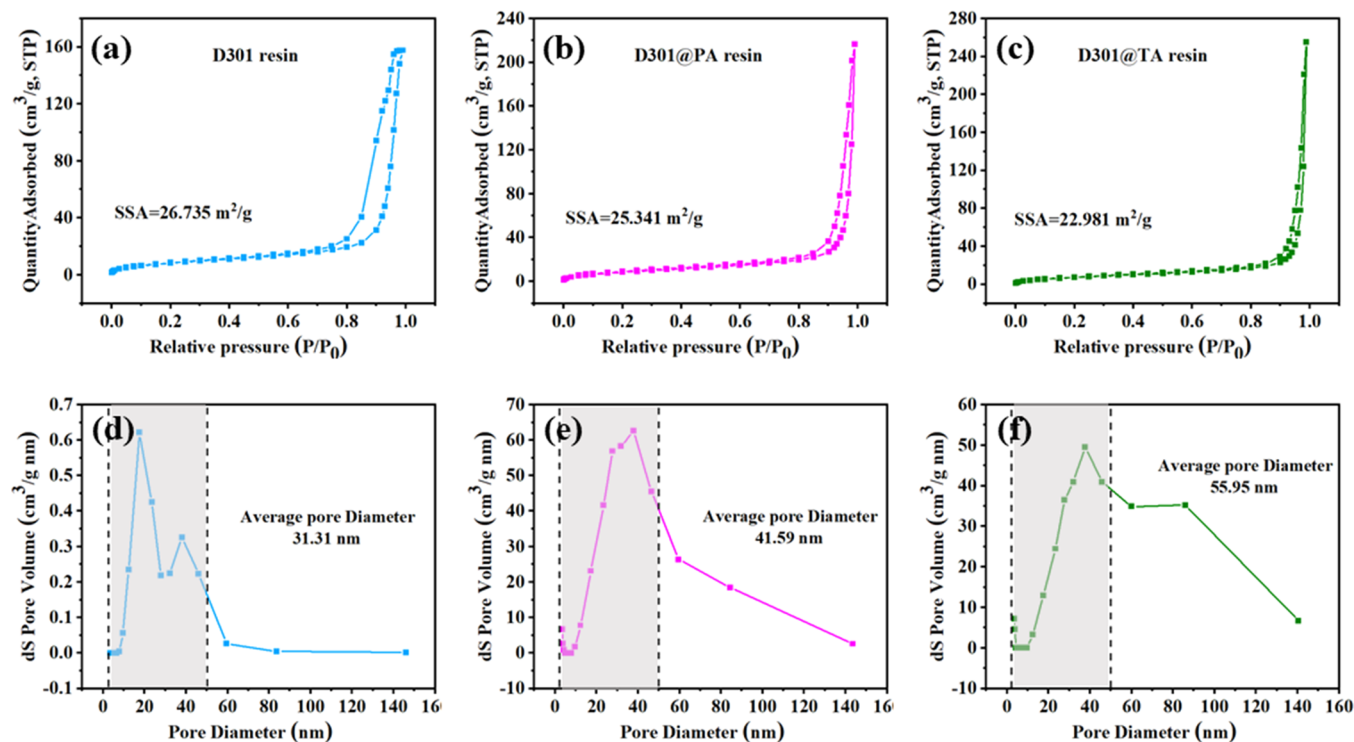**Figure 5.** SEM images of (a) D301, (b) D301@PA, and (c) D301@TA.

**Figure 6.** N$_2$ adsorption−desorption isotherm (a−c) and corresponding pore size distributions (d−f) of (a, d) D301, (b, e) D301@PA, and (c, f) D301@TA.
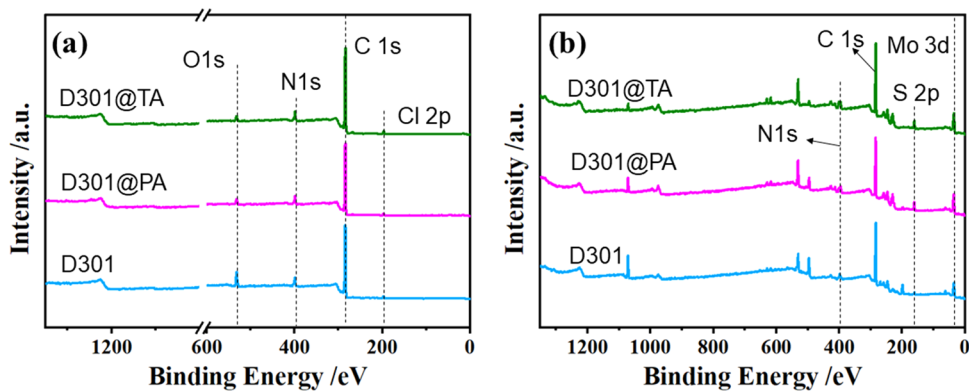


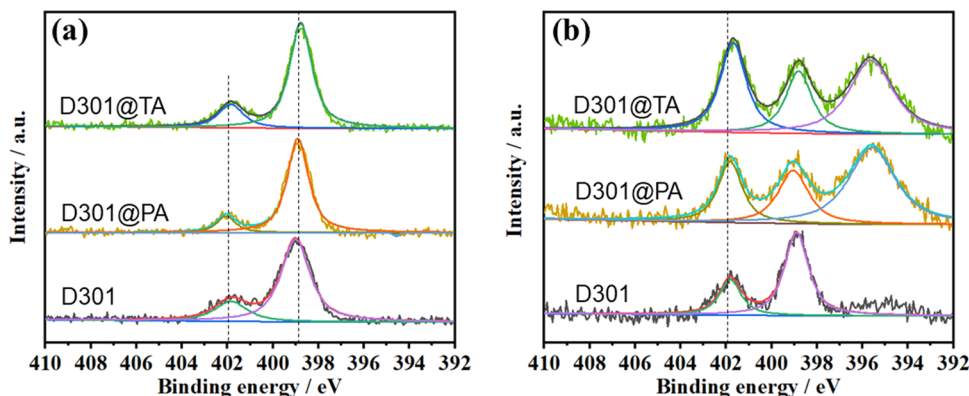**Figure 7.** XPS spectra of D301, D301@PA, and D301@TA (a) before and (b) after sorption of MoS$_4^{2-}$.



**Figure 8.** N spectra of D301, D301@PA, and D301@TA before (a) and after (b) sorption of MoS$_4^{2-}$.

material, and the sorption capacity of the sorbent cannot be described by the specific surface size alone. Actually, the

sorption capacity of the resins to MoS$_4^{2-}$ anions is mainly concentrated in the filling of micropores (below 2 nm). The

increase in the pore size distribution promotes faster passage to $MoS_4^{2-}$ molecules with a larger radius during the sorption process, so as to accelerate the sorption reaction between the adsorbents and $MoS_4^{2-}$ molecules.

**Ion Exchange.** The XPS full spectrum analysis of the adsorbent before and after sorption is performed. Figure 7a shows the XPS full spectrum results of the three adsorbents before adsorption, and Figure 7b shows the element distribution on the resin surface after adsorption. The resin is mainly composed of C, N, and Cl elements before adsorption. After adsorption, the Cl element disappeared and the distribution of Mo and S elements appeared. It is speculated that the resin undergoes anion exchange before and after adsorption, and the Cl⁻ anion on the resin was replaced by $MoS_4^{2-}$ in the solution species.

**Sorption Bonding.** To further analyze the changes before and after the sorption of D301, D301@PA, and D301@TA, Figure 8 shows a typical XPS N atom analysis. Among them, Figure 8a shows the N spectrum results of the three adsorbents before adsorption, and Figure 8b shows the N spectrum after adsorption. Through the comparison of N spectra before and after adsorption, the bonding relationship of the atoms can be accurately analyzed. First, Figure 8a shows the curves of D301, D301@PA, and D301@TA, where 402 and 399 eV are attributed to N⁺. Interestingly, compared with D301, the binding energies of D301@PA and D301@TA increased by 0.5 eV, which may be caused by their lattice defects. A quarter of the nitrogen ion positions in the crystal lattice are empty and have very high nitrogen ion conductivity, which leads to an increase in binding energy. After sorption, blue shifts of C−N bonds (from 402 to 401.6 eV and from 399 to 398.8 eV) are observed. Blue shifts can reduce the electron density around the N atoms, which makes it easier to obtain electrons to form N−$MoS_4^{2-}$ bonds. Fu et al.[26] reported that high-resolution XPS spectra of the nitrogen element reveal the blue shift of the pyridine N 1s peak (from 398.6 to 399.0 eV) and the ternary amine N 1s peak (from 400.4 to 401.0 eV) due to the stronger interaction between dipicolylamine groups and $MoS_4^{2-}$ ions.

**Reusability.** Compared with other sorption materials, polymer materials generally possess relatively high regeneration capacity in acid or alkaline elution. A 5 wt % sodium hydroxide solution was used as the eluent; the sorption data after five cycles are shown in Figure 9. It can be seen from Figure 9 that the sorption performance of the adsorbent has not changed significantly; therefore, the resin is cost-effective.
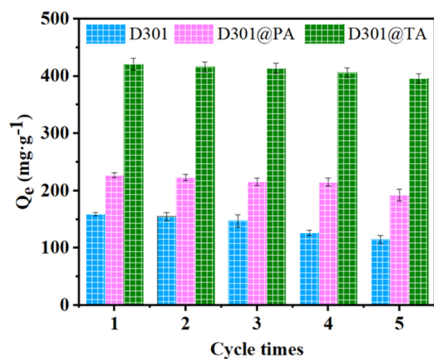


**Figure 9.** Regenerative performance of D301, D301@PA, and D301@TA at pH = 7.2 (contact time: 240 min and reaction temperature: 25 °C).

Considering the sorption capacity and sustainability, we infer that D301@TA has the best effect in large-scale industrial use.

**Stability.** To verify the stability of the resin, the morphology of the resin after five cycles of use was characterized, as shown in Figure 10. As can be seen, after five cycles, the pore structures of the modified resins ((b) D301@PA and (c) D301@TA) were obviously more regular than that of the resin before modification, which were also present before sorption. Moreover, compared with the resin before sorption, the pore structure has not changed. It is speculated that the stability of this pore structure is one of the main reasons for the resin to maintain its reusability.

## ■ CONCLUSIONS

In this study, two styrene-based sorbents, D301@PA and D301@TA, were synthesized by the hydrothermal method. Both sorbents use the styrene matrix as the skeleton, and different aminating agents N1923 and TOA are used as modifiers. They are uniformly modified on the surface and inside to increase the specific surface and pore size distribution, thereby increasing the sorption capacity of the resin. The experimental results show that the saturated sorption capacities of D301@PA and D301@TA reach 224 and 414 mg·g⁻¹ at 25 °C for 4 h. Moreover, by XPS characterization, the sorption mechanism of these two materials was deeply revealed. The whole sorption process can be divided into two steps. The first step was the ion exchange between the Cl⁻ anion on the resin and $MoS_4^{2-}$ in the solution. Then, the S atoms in $MoS_4^{2-}$ and the N atoms on the resin formed N−S bonds through electron transfer, and $MoS_4^{2-}$ anions were firmly adsorbed on the resins. By adjusting the experimental and characterization results, the modified resins D301@PA and D301@TA can be obtained and their sorption capacities to Mo were better than that of commercial D301 resin. Finally, further in-depth research, especially the reusable sorption−desorption experiments under working conditions, demonstrates that graft modification may be an effective method to further improve the capacity of the resin for practical industrial applications.

## ■ EXPERIMENTAL SECTION

**Materials.** The macroporous styrene matrix (D301) used in this study was purchased from Shanghai Kaiping Chemical Co., Ltd., China. N,N-Dimethylformamide (DMF, purity ≥ 99%), primary amine N1923 (PA, purity ≥ 95%), trioctylamine (TA, purity ≥ 95%), $Na_2WO_4 \cdot 2H_2O$ (purity ≥ 99.5%), and $Na_2MoO_4 \cdot 2H_2O$ (purity ≥ 99.5%) were kindly provided by Shanghai Macklin Biochemistry Co., Ltd., China. All of the other chemicals in this work were of AR grade. The stock solution containing tungsten and molybdenum was prepared by dissolving 66.4 g of $Na_2WO_4 \cdot 2H_2O$ and 2.42 g of $Na_2MoO_4 \cdot 2H_2O$ (both purity ≥ 99.9%) in 1 L of deionized water. Then, the solution was vulcanized ([S]/[Mo] = 6) for 2.5 h at 72 °C.

**Sorbent Preparation.** First, D301 resin was washed with distilled water until a neutral pH value was reached. Then, the resin was swelled in DMF (mass/vol = 1:4) and aminated in PA or TA (mass/vol = 1:4) to prepare D301@PA and D301@TA. The simple preparation procedure of two adsorbents is shown in Figure 11.

**Sorption Experiment.** Sorption experiments were performed by shaking 20 mL of raw solution with 0.02 g of amine resin in a 30 mL Erlenmeyer flask. To reduce the experimental
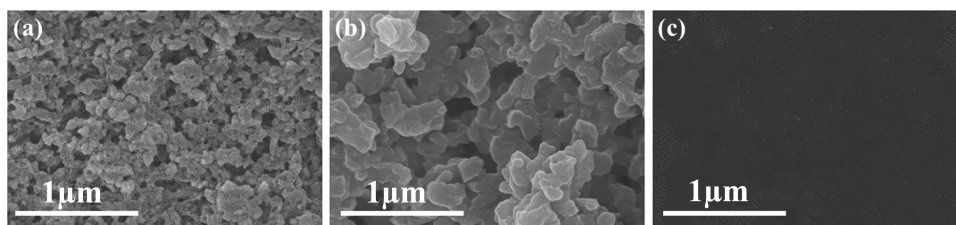
**Figure 10.** SEM images of (a) D301, (b) D301@PA, and (c) D301@TA after sorption of $MoS_4^{2-}$.
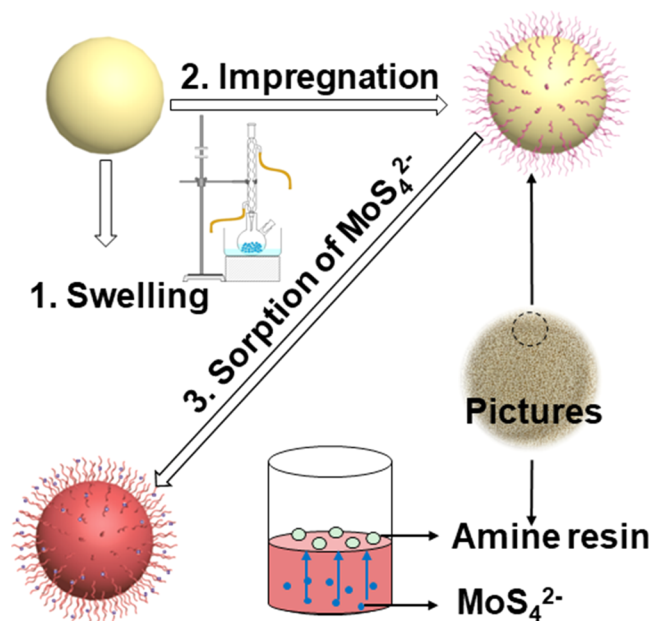


**Figure 11.** Schematic diagram for the preparation of D301@PA and D301@TA adsorbents and the $MoS_4^{2-}$ sorption experiment.

error, each group of experiments was conducted three times. Then, the metal concentration was determined by the standard deviation of the triplex analyzed values. The effects of pH values (5.8−11.8), reaction temperatures (25−75 °C), and reaction times (1−6 h) on the sorption capacity of the amine resin were studied. Then, the aqueous phase was separated to determine the concentration of the metal elements. The concentrations of W and Mo in the amine resin were calculated according to the rule of mass balance. The sorption capacity ($Q_e$), distribution ratio ($D$), and separation factor ($\beta$) were calculated according to

$$Q_e = \frac{(C_0 - C_e) \times V}{m} \qquad (2)$$

$$D = \frac{C_0 - C_e}{C_e} \qquad (3)$$

$$\beta = \frac{D_{Mo}}{D_W} \qquad (4)$$

where $C_0$ ($g \cdot L^{-1}$) is the raw concentration of Mo in the solution, and $C_e$ ($g \cdot L^{-1}$) is the Mo concentration after sorption equilibrium.

**Characterization.** A Thermo Scientific iCAP 6000 series inductively coupled plasma optical emission spectrometer (ICP-OES, PE) was used to confirm the concentration of metals in aqueous solution. Detailed information on the chemical states and electronic structures of Mo, S, N, C, and Cl

on the surface was obtained via X-ray photoemission spectroscopy (XPS, Thermo Fisher Scientific). The N 1s spectra were measured using a KRATOS Axis Ultra X-ray photoelectron spectrometer equipped with a monochromatic Al Kα source and a charge compensation system. During data collection, the step size was set to 0.05 eV, and 10 scans for each sample were averaged. All NMR spectra were recorded on a Bruker Inc., Switzerland ($^{13}$C: 400 MHz). Scanning electron microscopy (SEM) was performed on a Gemini SEM 300 (Germany) to study the morphologies of the three materials before and after modification. The $N_2$ adsorption−desorption isotherms of the three materials were tested using an ASAP 2020 apparatus utilizing BET and BJH models (Quantachrome Instruments).

**DFT Calculations.** Density functional theory (DFT) is a quantum mechanical method for studying the distribution of electrons in multielectron systems.[25,27,28] It uses electron density instead of wave functions as the basic quantity for the study, simplifying the interaction between electrons in multielectron systems. Some scholars have used the DFT method to calculate the ground-state electronic structures of resin molecules.[29,30] In this study, the DMol3 module in Materials Studio (Accelrys) was used for calculation, and the exchange−correlation functional of the calculation process selects the PBE functional under the generalized gradient approximation (GGA).

## ■ ASSOCIATED CONTENT

**ⓈⒾ Supporting Information**

The Supporting Information is available free of charge at https://pubs.acs.org/doi/10.1021/acsomega.1c06257.

> Detailed discussion about experimental data under different reaction temperatures; pH values; contact times; and raw concentrations of Mo in the solution (PDF)

## ■ AUTHOR INFORMATION

**Corresponding Author**

> **Xiaoli Xi** − *Collaborative Innovation Center of Capital Resource-Recycling Material Technology, Beijing University of Technology, Beijing 100124, China; Key Laboratory of Advanced Functional Materials, Ministry of Education, Faculty of Materials and Manufacturing, Beijing University of Technology, Beijing 100124, China;* ⓘ orcid.org/0000-0002-7669-4542; Phone: 86-10-67391536; Email: xixiaoli@bjut.edu.cn

**Authors**

> **Fan Guo** − *Collaborative Innovation Center of Capital Resource-Recycling Material Technology, Beijing University of Technology, Beijing 100124, China*

**Liwen Ma** − *Collaborative Innovation Center of Capital Resource-Recycling Material Technology, Beijing University of Technology, Beijing 100124, China; National Engineering Laboratory for Industrial Big-Data Application Technology, Beijing University of Technology, Beijing 100124, China*

**Zuoren Nie** − *Collaborative Innovation Center of Capital Resource-Recycling Material Technology, Beijing University of Technology, Beijing 100124, China; Key Laboratory of Advanced Functional Materials, Ministry of Education, Faculty of Materials and Manufacturing and National Engineering Laboratory for Industrial Big-Data Application Technology, Beijing University of Technology, Beijing 100124, China*

Complete contact information is available at:
https://pubs.acs.org/10.1021/acsomega.1c06257

**Notes**

The authors declare no competing financial interest.

## ■ ACKNOWLEDGMENTS

## ■ REFERENCES

(1) Li, J.; Cao, Z.; Zeng, L.; Xu, M.; Zhang, G.; Li, Q.; Guan, W. A New Recyclable Sulfurizing Reagent for Mo-S Complexes and Separation of Molybdenum from Tungstate Solutions. *Sep. Purif. Technol.* **2019**, *212*, 490−496.

(2) Bettinardi, D. J.; Paulenova, A.; Tkac, P. Speciation of Molybdenum(VI) in Chloride Media at Elevated Mo Concentrations. *ACS Omega* **2020**, *5*, 23786−23792.

(3) Pan, F.; Liu, J.; Du, Z.; Zhu, Q.; Zhang, M.; Yan, D.; Li, S. Reaction Process of WC Prepared under a CO Atmosphere in a Fluidized Bed. *Ind. Eng. Chem. Res.* **2021**, *60*, 162−172.

(4) Zhao, B.; Liang, Y.; Yan, W.; Liu, L.; Dong, J. A Facile Approach to Tune WO$_x$ Species Combining Pt Catalyst for Enhanced Catalytic Performance in Glycerol Hydrogenolysis. *Ind. Eng. Chem. Res.* **2021**, *60*, 12534−12544.

(5) Du, J.; Li, J.; He, D.; Xu, M.; Zhang, G.; Cao, Z.; Wu, S. Green Separation and Recovery of Molybdenum from Tungstate Solution Achieved by Using a Recyclable Vulcanizing Agent. *J. Cleaner Prod.* **2021**, *278*, No. 123930.

(6) Li, Z.; Lu, J.; Wu, S.; Zhang, G.; Guan, W.; Zeng, L.; Li, Q.; Cao, Z. Sustainable Extraction and Complete Separation of Tungsten from Ammonium Molybdate Solution by Primary Amine N1923. *ACS Sustainable Chem. Eng.* **2020**, *8*, 6914−6923.

(7) Quijada-Maldonado, E.; Sánchez, F.; Pérez, B.; Tapia, R.; Romero, J. Task-Specific Ionic Liquids as Extractants for the Solvent Extraction of Molybdenum(VI) from Aqueous Solution Using Different Commercial Ionic Liquids as Diluents. *Ind. Eng. Chem. Res.* **2018**, *57*, 1621−1629.

(8) Nguyen, T. H.; Lee, M. S. Separation of Molybdenum(VI) and Tungsten(VI) from Sulfate Solutions by Solvent Extraction with LIX 63 and PC 88A. *Hydrometallurgy* **2015**, *155*, 51−55.

(9) Huo, G.; Peng, C.; Song, Q.; Lu, X. Tungsten Removal from Molybdate Solutions Using Ion Exchange. *Hydrometallurgy* **2014**, *147−148*, 217−222.

(10) Tkac, P.; Momen, M. A.; Breshears, A. T.; Brown, M. A.; Vandegrift, G. F. Molybdenum(VI) Coordination in Tributyl Phosphate Chloride Based System. *Ind. Eng. Chem. Res.* **2018**, *57*, 5661−5669.

(11) Padh, B.; Rout, P. C.; Mishra, G. K.; Suresh, K. R.; Ramachandra Reddy, B. Recovery of Nickel and Molybdate from Ammoniacal Leach Liquors of Spent HDS Catalysts Using Chelating Ion Exchange Resin. *Hydrometallurgy* **2019**, *184*, 88−94.

(12) Banerjee, P.; Ansari, S. A.; Mohapatra, P. K.; Egberink, R. J. M.; Ramasubramanium, S.; Patil, C. B.; Huskens, J.; Verboom, W. Highly Efficient Europium(III) Uptake with an Extraction Chromatographic Resin Containing a Unique Multiple Diglycolamide Ligand with a Tetraaza-12-crown-4 Scaffold. *Ind. Eng. Chem. Res.* **2021**, *60*, 2613−2624.

(13) Zhao, Z.; Zhang, J.; Chen, X.; Liu, X.; Li, J.; Zhang, W. Separation of Tungsten and Molybdenum Using Macroporous Resin: Equilibrium Adsorption for Single and Binary Systems. *Hydrometallurgy* **2013**, *140*, 120−127.

(14) Zang, Y.; Yue, Q.; Kan, Y.; Zhang, L.; Gao, B. Research on Adsorption of Cr(VI) by Poly-epichlorohydrin-dimethylamine (EPI-DMA) Modified Weakly Basic Anion Exchange Resin D301. *Ecotoxicol. Environ. Saf.* **2018**, *161*, 467−473.

(15) Awual, M. R. A Novel Facial Composite Adsorbent for Enhanced Copper(II) Detection and Removal from Wastewater. *Chem. Eng. J.* **2015**, *266*, 368−375.

(16) Awual, M. R. Novel Nanocomposite Materials for Efficient and Selective Mercury Ions Capturing from Wastewater. *Chem. Eng. J.* **2017**, *307*, 456−465.

(17) Wu, X. S.; Zhang, G. Q.; Zeng, L.; Guan, W. G.; Wu, S. X.; Li, Z. H.; Zhou, Q.; Zhang, D.; Qing, J. L.; Long, Y. C.; Li, J.; Li, Q. G.; Cao, Z. Y.; Xiao, L. S. Continuous Solvent Extraction Operations for the Removal of Molybdenum from Ammonium Tungstate Solution with Quaternary Ammonium Salt Extractant. *Hydrometallurgy* **2020**, *195*, No. 105401.

(18) Zheng, Z.; Jia, Q.; Xie, X.; Zheng, X.; Yao, C.; Xiong, C.; Jiang, J. Removal and Recovery of Mo(IV) from Aqueous Solutions by D201 Resin: Adsorption and Column Studies. *Asian J. Chem.* **2014**, *26*, 393−395.

(19) Hassanpour, S.; Taghizadeh, M. Rapid and Selective Separation of Molybdenum Ions Using a Novel Magnetic Mo(VI) Ion Imprinted Polymer: A Study of the Adsorption Properties. *RSC Adv.* **2016**, *6*, No. 100248.

(20) Masry, B. A.; Daoud, J. A. Sorption Behavior of Tungsten and Molybdenum on TVEX-TOPO Resin from Nitric Acid Solution. *J. Chem. Technol. Biotechnol.* **2021**, *96*, 1399−1410.

(21) Tuchowska, M.; Muir, B.; Kowalik, M.; Socha, R. P.; Bajda, T. Sorption of Molybdates and Tungstates on Functionalized Montmorillonites: Structural and Textural Features. *Materials* **2019**, *12*, No. 2253.

(22) Liansheng, X.; Qixiu, Z.; Bofan, G.; Shaoying, H. Separation of Molybdenum from Tungstate Solution by a Combination of Moving Packed Bed and Fluid Bed Ion-exchange Techniques. *Int. J. Refract. Hard Met.* **2001**, *19*, 145−148.

(23) Lai, W.; Zhang, K.; Shao, P.; Yang, L.; Ding, L.; Pavlostathis, S. G.; Shi, H.; Zou, L.; Liang, D.; Luo, X. Optimization of Adsorption Configuration by DFT Calculation for Design of Adsorbent: A case study of palladium ion-imprinted polymers. *J. Hazard. Mater.* **2019**, *379*, No. 120791.

(24) Liu, Y.; Liu, R.; Ding, W.; Wang, D. Evaluation of Influencing Factors in Tetravalent Uranium Complex-Mediated CO$_2$ Functionalization by Density Functional Theory. *J. Phys. Chem. A* **2020**, *124*, 2683−2693.

(25) Montoro, O. R.; Tortajada, J.; Lobato, A.; Baonza, V. G.; Taravillo, M. Theoretical (DFT) and Experimental (Raman and FTIR) Spectroscopic Study on Communic Acids, Main Components of Fossil Resins. Spectrochim. *Spectrochim. Acta, Part A* **2020**, *224*, No. 117405.

(26) Fu, W.; Ji, G.; Chen, H.; Yang, S.; Guo, B.; Yang, H.; Huang, Z. Molybdenum Sulphide Modified Chelating Resin for Toxic Metal Adsorption from Acid Mine Wastewater. *Sep. Purif. Technol.* **2020**, *251*, No. 117407.

(27) Jing, Y.; Chen, J.; Chen, L.; Su, W.; Liu, Y.; Li, D. Extraction Behaviors of Heavy Rare Earths with Organophosphoric Extractants: The Contribution of Extractant Dimer Dissociation, Acid Ionization, and Complexation. A Quantum Chemistry Study. *J. Phys. Chem. A* **2017**, *121*, 2531−2543.

(28) Rahuman, M. H.; Muthu, S.; Raajaraman, B. R.; Raja, M.; Umamahesvari, H. Investigations on 2-(4-Cyanophenylamino) Acetic Acid by FT-IR,FT-Raman, NMR and UV-Vis spectroscopy, DFT (NBO, HOMO-LUMO, MEP and Fukui function) and Molecular Docking Studies. *Heliyon* **2020**, *6*, No. e04976.

(29) Zhang, N.; Königsberger, E.; Duan, S.; Lin, K.; Yi, H.; Zeng, D.; Zhao, Z.; Hefter, G. Nature of Monomeric Molybdenum(VI) Cations in Acid Solutions Using Theoretical Calculations and Raman Spectroscopy. *J. Phys. Chem. B* **2019**, *123*, 3304−3311.

(30) Song, Y. Y.; Dong, B.; Wang, S. W.; Wang, Z. R.; Zhang, M.; Tian, P.; Wang, G. C.; Zhao, Z. Selective Oxidation of Propylene on $Cu_2O(111)$ and $Cu_2O(110)$ Surfaces: A Systematically DFT Study. *ACS Omega* **2020**, *5*, 6260−6269.